© 2020. Published by The Company of Biologists Ltd | Journal of Experimental Biology (2020) 223, jeb221010. doi:10.1242/jeb.221010

RESEARCH ARTICLE

The control of nocifensive movements in the caterpillar *Manduca sexta*

Ritwika Mukherjee[1], Daniel P. Caron[1], Timothy Edson[2] and Barry A. Trimmer[1,*]

ABSTRACT

In response to a noxious stimulus on the abdomen, caterpillars lunge their head towards the site of stimulation. This nocifensive 'strike' behavior is fast (~0.5 s duration), targeted and usually unilateral. It is not clear how the fast strike movement is generated and controlled, because caterpillar muscle develops peak force relatively slowly (~1 s) and the baseline hemolymph pressure is low (<2 kPa). Here, we show that strike movements are largely driven by ipsilateral muscle activation that propagates from anterior to posterior segments. There is no sustained pre-strike muscle activation that would be expected for movements powered by the rapid release of stored elastic energy. Although muscle activation on the ipsilateral side is correlated with segment shortening, activity on the contralateral side consists of two phases of muscle stimulation and a marked decline between them. This decrease in motor activity precedes rapid expansion of the segment on the contralateral side, presumably allowing the body wall to stretch more easily. The subsequent increase in contralateral motor activation may slow or stabilize movements as the head reaches its target. Strike behavior is therefore a controlled fast movement involving the coordination of muscle activity on each side and along the length of the body.

KEY WORDS: Motor control, Pain, Strike behavior, Soft bodied, Neuromechanics

INTRODUCTION

In articulated animals with stiff skeletons, movement is produced by muscles working antagonistically around joints to produce directionally constrained motions, and structural levers to allow the mechanical exchange of force and displacement. Because the joints have clearly defined translational and rotational degrees of freedom, the position and orientation of the limbs can be estimated by the joint angles and the location of other body parts (Colobert et al., 2006; Holmes et al., 2006).

In contrast, soft animals move by controlling body deformations instead of actuated joints and exploit changes in conformation for different types of motion. Soft muscular hydrostats, such as octopus arms, squid tentacles, elephant trunks, frog tongues and annelids, move by maintaining constant volume and activating selected muscle groups to change shape and distribute forces through hydrostatic pressure (Kier and Schachat, 1992; Kier and Smith, 1983, 1985; Kier and Stella, 2007; Nishikawa et al., 1999; Yekutieli et al., 2005). Typically, their circumferential muscles operate antagonistically to the longitudinal muscles to control extension and shortening (Kristan et al., 2005), a mechanism that depends on a largely incompressible body cavity and relatively high internal pressures (Quillin, 1998; Skierczynski et al., 1996; Wilson et al., 1996). Internal pressure in hydrostats produces rigidity and posture, which allows muscle contractions to direct forces better. Behaviors with high body curvature are especially likely to use elevated internal pressures to generate forces. For example, earthworms can generate radial pressures up to almost 200 kPa during crawling (Ruiz et al., 2015). Muscle contraction is correlated with the development of internal pressure, which creates high forces resulting in powerful movements (Westneat et al., 1998; Wilson et al., 1996).

Caterpillars are entirely soft but they are not muscular hydrostats. They have distinctive body segments, but these segments are not internally separated by septa, as in earthworms. Instead, they have an open hemocoel through which the gut and body fluids can move freely during locomotion (Simon et al., 2010a,b). Caterpillars also do not maintain a constant volume, as they have spiracles that allow gas exchange and air-filled trachea that permeate all the tissues, making the body compressible. This compressibility might explain why the baseline body pressure is low (<2 kPa) (Lin et al., 2011) and even during vigorous body movements such as strike behavior, the hemolymph pressure does not exceed 4 kPa. Pressure changes are not used to actively control proleg movements (Mezoff et al., 2004).

Although caterpillars generally move slowly, most can move quickly in response to a brief noxious stimulus. In *Manduca sexta*, this consists of a rapid lateral bend that brings the head and mandibles close to an affected site on the posterior abdomen. The movement, called a strike response, is used to startle or otherwise remove a potential attacker (Walters et al., 2001). It can be provoked by strong mechanical stimuli (such as a pinch) (McMackin et al., 2016; Tabuena et al., 2017), or by potentially harmful thermal stimuli (Frings, 1945; Mukherjee and Trimmer, 2019).

Strike responses are targeted to the stimulus site and involve a rapid shortening of the ipsilateral (same side as the stimulus) margin of the abdominal body segments and an expansion of the opposite side of each segment. For strikes directed at a lateral posterior stimulus, most of the movement is in the lateral plane with only a small lifting component in the dorsal direction. Little is known about the neural or muscular mechanisms underlying this behavior. Each abdominal segment in *M. sexta* contains approximately 50 muscles (Levine and Truman, 1985). Many of these are small muscles, just under the cuticle, attached to local apodemes within each body segment (usually referred to as 'external' muscles). Large muscles (the 'internal' muscles) span each segment longitudinally and are thought to be responsible for shortening each body segment (Fig. 1). A small number of muscles are arranged obliquely but there are no circumferential muscles such as those found in annelids and mollusks.

[1]Tufts University, Department of Biology, 200 Boston Avenue, Suite 2600, MA 02155, USA. [2]Department of Chemistry and Biochemistry, Bates College, 2 Andrews Road, Lewiston, ME 04240, USA.

*Author for correspondence (barry.trimmer@tufts.edu)

R.M., 0000-0003-2815-6229; D.P.C., 0000-0002-1500-8713; B.A.T., 0000-0003-1782-7373

Received 30 December 2019; Accepted 1 July 2020

Journal of Experimental Biology (2020) 223, jeb221010. doi:10.1242/jeb.221010

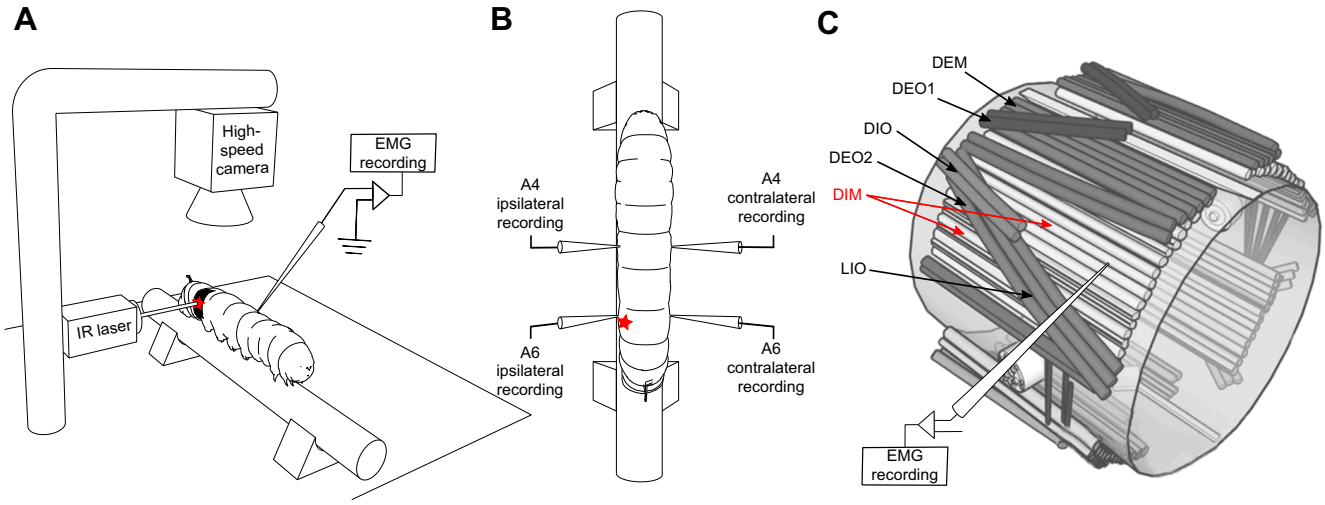

Fig. 1. Design of the experimental setup. (A) An infrared (IR) laser was placed 30 cm from one side of the caterpillar and a high-speed camera was positioned 25 cm above the caterpillar. The IR laser generated a focused heat stimulus to evoke a strike response towards the stimulus site (marked by a red star). In addition, electromyography (EMG) recordings were collected during an ongoing strike response. (B) EMG recordings were collected from the dorsal interior medial (DIM) muscles in abdominal segments A4 and A6 on either side of the caterpillar. A strike response was unilateral with the head bending towards the stimulus site on the ipsilateral side. The EMGs were recorded using stainless steel bipolar electrodes and the signals were amplified (×200 gain) and digitalized at 30 kHz. (C) Schematic diagram of the major muscles in abdominal segments A4 and A6. Recordings were made from the largest dorsal longitudinal muscle (DIM, labeled with red arrows). Nearby muscles also responsible for segment shortening include the DEM (dorsal exterior muscle), DIO (dorsal interior oblique), DEO1,2 (dorsal exterior oblique) and LIO (lateral interior oblique).

Given this arrangement of muscles, there are several possible mechanisms for generating a fast and targeted strike movement. For example, many fast movements in animals are generated by preloading mechanical structures and then triggering the release of stored elastic energy (Patek et al., 2011). In *M. sexta* this could be accomplished by a pre-strike co-contraction of the longitudinal muscles on both sides, followed by body wall buckling that collapses the abdomen to one side. Targeting might be directed by specific muscles controlling the site of buckling but these structural instabilities would need to be highly reproducible to account for the accuracy of the strike (van Griethuijsen et al., 2013). Alternatively, strikes could be controlled directly by differential muscle activation. This could be broadly coordinated throughout the body, restricted to one side, or confined to the stimulated region of the abdomen.

Here, we describe the timing of the strike response by tracking length changes on each side of each abdominal segment with millisecond time resolution. We show that there are asymmetrical changes in the contraction and expansion of the abdomen and relate this to the degree of longitudinal muscle activation on each side of two abdominal segments. We found a propagating bending pattern during a strike that was accompanied by a wave of muscle activity from anterior to posterior on both sides of the body. The ipsilateral motor activity was continuous and correlated with the segment bending towards the side of the stimulus. We did not find strong evidence for a pre-strike muscle loading phase that would be expected for an 'uncontrolled' strike mechanism but, instead, the timing of muscle activation is consistent with the ipsilateral muscles directly driving the bending movement.

Motor activity on the contralateral side (opposite side to the stimulus) was phasic, with increased activity at the beginning and end of the behavior and a marked decline between them. The intermediate decrease in contralateral motor activity precedes a rapid expansion of that side suggesting that it allows the contralateral side to stretch more easily. The subsequent increase in contralateral motor activation may play a role in slowing or stabilizing the movement as the head reaches its target. Strike behavior is therefore a controlled fast movement involving the coordination of muscle activity on each side and along the length of the body.

MATERIALS AND METHODS

Animals

The experiments used early 5th instar larvae of tobacco hornworm *Manduca sexta* (Linnaeus 1763). The animals were raised at a constant temperature of 27°C on an artificial diet on a 17 h:7 h light: dark cycle following the maintenance protocol as described by Bell and Joachim (1978).

Noxious heat stimuli

Infrared (IR) lasers (Class 3B Laser; 808 nm, 400 mW) were used to deliver localized and reproducible thermal stimuli. A segment of the cuticle was coated with an approximately 200–300 µm thick layer of black paint (Rustoleum, flat black, oil modified alkyd), because the cuticle is IR reflective. The caterpillars were mounted on a wooden stick, with lasers positioned 30 cm away. The laser was activated to generate a local hotspot by a 200 ms square wave pulse generated by a USB data acquisition card (National Instruments USB-9263, 4-Ch ±10 V 16-Bit Analog Output, National Instruments, Austin, TX, USA) using LabVIEW (Elliott et al., 2007). The peak local temperature reached a maximum of 52°C.

Electromyography of natural strike response

Bipolar electromyography (EMG) electrodes were used to record from two abdominal segments of the caterpillar, A4 and A6, during a strike response. The bipolar electrodes were fabricated by soldering a pair of intertwined 114.3 µm coated (50.8 µm bare) diameter stainless steel (A-M Systems, Inc., cat. no. 790600) wires to the terminals of a male two-pin connector. The tips of the wires were burnt to remove coating on the ends and increase the surface area of contact with muscles. A surgical needle was used to make a small hole on the dorsal side of the segments of an anesthetized animal, and the electrode was inserted through the cuticle into the dorsal

interior medial (DIM) muscles. The DIM muscles are the biggest dorsal longitudinal muscles in every segment and DIM muscles in each hemi-segment are innervated by two motor neurons (Levine and Truman, 1985). Because a strike response is typically unilateral, the ipsilateral and contralateral side of A4 and A6 had unique movement profiles. So, those sites were selected for recording muscle activity patterns during a strike response (Fig. 1B). Only two or three of these four sites were simultaneously recorded during any strike response.

The electrode wires were connected to the inputs of a 16-channel RHD 2216 amplifier board (Intan Technologies LLC., Los Angeles, CA, USA; http://intantech.com). Four channels of the amplifier were employed to acquire signals from four sites on the caterpillar. A fifth channel was used to record the time of the IR pulse that was later used to synchronize the time of the EMG signals with the kinematic data. The signals were acquired at 30 kHz and amplified at ×200 gain, high-pass filter of 1 Hz and low-pass filtered at 7.5 kHz. The recordings were sensitive to signals of the order of microvolts. The digital output generated by the Intan evaluation board (USB interface board; intantech.com/files/Intan_RHD2000_eval_system) was saved as an RHD data file. The RHD file was converted to a text file and analyzed in MATLAB (Mathworks, Natick, MA, USA). EMGs can be resolved into electrical spikes representing general neural activity (Dominick and Truman, 1986). Each spike in the EMG traces was an excitatory junction potential (EJP) that was detected as it exceeded an amplitude threshold and the activity was represented by rasters of the spikes.

High-speed videography of strike response

An overhead high-speed camera (Phantom VEO 640L monochrome, Vision Research, Wayne, NJ, USA) with a macro lens (Nikon AF NIKKOR 35 mm f/2D Lens, Nikon Company, Tokyo, Japan) was used for recording strike behavior at 1000 frames s^{-1} (Movie 1). The field of view (dorsal aspect, approximately 9 cm×7 cm; 1280×960 pixels) was calibrated using a 1 mm grid with a calculated resolution of 71.63 µm $pixel^{-1}$. The duration of a strike response was defined as the time from the beginning of head movement to when the head contacted the body.

For the combined kinematic and electromyographic analyses of the strike response, measurements of muscle activity and video recordings were made simultaneously (n=13 insects). Up to six strike responses were recorded from each insect with simultaneous muscle recordings from at least two out of four sites of interest selected for analysis. Because of the different combinations of the four sites (A4 and A6, ipsilateral and contralateral) of recordings, there were different sample sizes of kinematic and muscle recordings from A4 ipsilateral (n=13), A4 contralateral (n=11), A6 ipsilateral (n=16) and A6 contralateral (n=19).

Experimental design

The IR-laser pulse was focused on a small region of the body wall slightly dorsal to the spiracle. The stimulus was visualized using an IR-fluorescent phosphor card or by directly observing the beam in the (IR-sensitive) camera view (Fig. 1A). Brief stimuli (up to ∼150 ms) to naive larvae evoked local twitches but rarely caused a strike. Longer stimuli (200 ms) reliably evoked strike responses (Mukherjee and Trimmer, 2019).

Data analysis

Kinematic data analysis

The kinematic data were used to evaluate the duration and mechanics of the strike response. Changes in the shapes of all abdominal segments were tracked during a strike response from the videos. To do so, the four corners of each abdominal segment were tracked frame by frame during a strike response when stimulated at A6 (n=4). With the digitized data, the ipsilateral contractions and contralateral expansions were described across the abdomen of the caterpillar during a strike response. The kinematic data from segments A4 and A6 were used to compare the shape changes from the resting pre-strike segment lengths. Finally, the normalized kinematic data were combined with muscle activity profiles to describe the relationship between muscle activation and changes in segment length.

EMG data analysis

Once imported as text files from the amplifier, the EMG signals were passed through a band-pass filter with low cut-off frequency at 20 Hz and high cut-off frequency at 1000 Hz using LabChart (LabChart 7Pro v7.3.4, ADInstruments Inc., Colorado Springs, CO, USA). Using the synchronized marker of the IR pulse from the amplifier, the EMG signals of interest were carefully marked from the beginning of the stimulus till the time of the end of a strike response. The selected EMG data from each strike response were temporally normalized to the strike duration. EMG and kinematics of different strike durations were compared after normalization by dividing the absolute time by the strike duration.

From the normalized EMG traces from each recording site, spikes were detected with an amplitude threshold. These spikes were analyzed as time stamps in the form of rasters of neural spike trains. The spike trains were temporally aligned for each recording site. The probability distributions of spike occurrences for ipsilateral and contralateral sites of A4 and A6 were obtained by dividing each time-normalized strike into 80 time bins (from −1 to 1 of normalized strike duration, corresponding to approximately 13.5 ms each) and marking the presence of a spike in a bin as 1 and the absence as 0. The bin duration was short enough that, at the maximum spike rate (∼50 Hz), only a single EJP could occur in each bin. The probability of a spike occurring in each time bin was calculated as the proportion of trials containing a spike (100%=1). The start of EMG activity was measured by differentiating the binned spike distributions (using total spike numbers) and checking for the first local maxima.

The spike probability distributions were smoothed in JMP (JMP statistical software, SAS Institute Inc., Cary, NC, USA) for further analysis. These spike probability distributions were temporally correlated with the kinematic distributions. The EMG activity occurring after the end of the strike response to bring the insect back to the resting state was not considered within the scope of this study.

Peak muscle force and the rate of shortening increase with higher stimulation frequency (Aubert et al., 1951). Therefore, the spike probability distributions were used as a proxy for muscle activity and these were compared with the speed of contraction and expansion of the segments calculated as the first derivative of the length with respect to time. In addition to representing the variable EMG data as spike occurrence probabilities, ‘central spike trains’ were constructed for all four sets of rasters of neural spikes. The spike trains were mapped into a space of functions through a causal exponential filter. The average of those functions was mapped back to a spike train by finding a sequence whose filtered function was close to the average function (Julienne and Houghton, 2013). This central spike train algorithm has been shown to be better than the medoid spike train in representing groups of variable rasters.

Statistics

The dependence of segment length changes on the normalized strike duration or time was estimated using generalized linear mixed

Journal of Experimental Biology (2020) 223, jeb221010. doi:10.1242/jeb.221010

models (GLMMs) through lme4::glmer (Bates et al., 2015 preprint) in program R (http://www.R-project.org). The fixed effects of normalized duration of strike, site of stimulation and their interaction were evaluated using lmtest::lrtest (Zeileis and Hothorn, 2002) and car::Anova (Fox et al., 2013). Individuals were treated as a random effect to account for any unintentional heterogeneity in our recordings. All models were evaluated using Akaike information criterion (AIC) using bbmle::ICtab (https://CRAN.R-project.org/package=bbmle).

The relationship of the segment expansion and contraction speeds to the ipsilateral and contralateral EMG activity patterns was also examined using GLMMs through lme4::glmer. The models were evaluated using AIC.

Other statistical tests such as estimated marginal means Tukey method and Welch's two sample *t*-test were implemented to compare numerical groups and one-sample Chi-squared test on variance was used to measure variance of the target site.

RESULTS

Caterpillars respond to noxious thermal stimuli

Manduca sexta strike when a very brief (200 ms), localized (650–700 µm diameter) thermal stimulus is applied to the dorsal lateral surface of the abdomen (Fig. 1). An example of a strike response was used to demonstrate the movement temporally (Fig. 2A). Average strike duration (from the beginning of the movement to contact with the stimulation site) was 541.5±50.35 ms (mean± s.e.m.) (Mukherjee and Trimmer, 2019). Strike duration was not significantly different between the insects stimulated at A4 and A6 (Welch's two-sample *t*-test, t=0.35, P=0.72; average strike duration: 549.3±25.13 and 534.6±42.13 ms for A4 and A6, respectively). The strike response was targeted (Welch's two-sample *t*-test, P=4.177e–10, n=18 trials across 8 animals) with higher accuracy at the A6 stimulation site than at the A4 site (one-sample Chi-squared test on variance with the null hypothesis that variance is 1: target A4: $\chi^2_{variance}$=8.02, d.f.=17, estimated variance with confidence interval=0.472 [0.266, 1.061], P=0.068; target A6: $\chi^2_{variance}$=5.27, d.f.=17, estimated variance with confidence interval=0.309 [0.174, 0.696], P=0.0062) (Fig. 2B,C). The accuracy was described by the variance of the target site from the actual mid-point of the segment of interest. Higher dispersion in the target sites indicated lower accuracy in targeting.

Morphological changes in abdominal segments during a strike response

The morphological changes across the insect were tracked across all abdominal segments on the ipsilateral and contralateral sides of all abdominal segments. Length changes during a strike differed between abdominal segments with a significant dependence on time, the segment of interest and their interaction [ANOVA (Type II test); Change in length of all segments~Time+Segment+Time: Segment; P<2.2e−16; n=4 animals]. All segments showed different contraction and expansion profiles across the body (estimated marginal means, ipsilateral versus contralateral length changes in A1–A5: P<0.001, changes in A6: P=0.003, n=4 animals) (Fig. 3B).

Abdominal segment A4 underwent a bigger change in length than the posterior segment A6 both ipsilaterally (estimated marginal means Tukey method, z-ratio=−136.8, P<0.001) and contralaterally (estimated marginal means Tukey method, z-ratio=82.3, P<0.001) (Fig. 3). Linear mixed models were run to evaluate the dependence of segment expansion and contraction on time (duration of strike) and the segment type (A4 or A6). The length change profiles depended significantly on both predictor variables and their interaction (model with the lowest AIC won, ANOVA Type II; χ^2=676.7, P<2.2e–16; association confirmed by likelihood-ratio (LR) test of additive versus interaction model: χ^2=958.2, d.f.=−3, P<2.2e–16; n=13 A4 ipsilateral; n=11 A4 contralateral; n=16 A6 ipsilateral; n=19 A6 contralateral; n=13 animals).

EMG profiles from A4 and A6 have differential activation patterns with a temporal lag for A6

The rasters of neural spikes (i.e. EJPs) were variable for all four recording sites (Fig. 4). The EMG data (n=13 animals) showed differential activity across segments. The muscle activity started earlier in the anterior segment (least square means test, P<0.015) with contralateral activity generally starting before ipsilateral activity (least square means test, P<0.001).

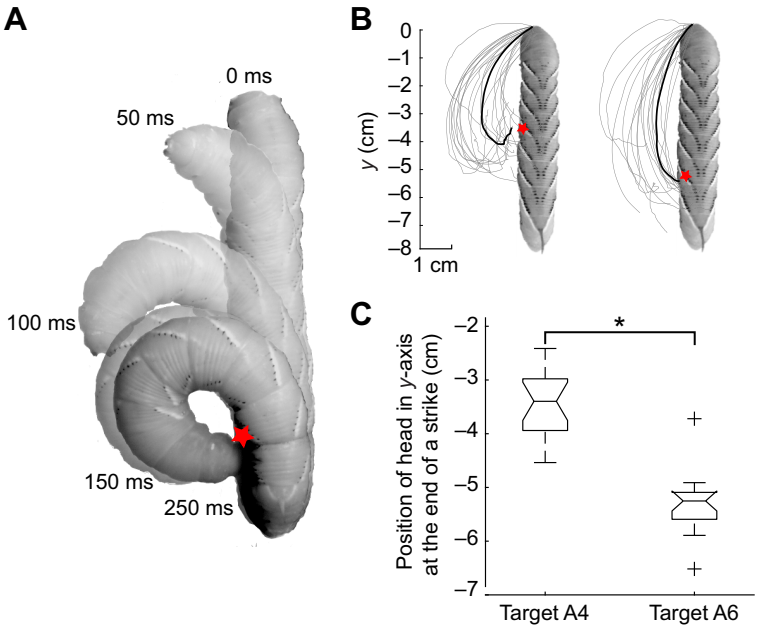

Fig. 2. Characterization of a strike response evoked by a noxious stimulus. (A) Time sequence of the strike response that occurred within 250 ms. The caterpillar was stimulated at A6 (red star). (B) Upon stimulation at two different target sites, A4 and A6 (indicated by red stars), the head followed different trajectories to reach the target site (n=18 for each stimulation site across 8 animals). (C) Notched box plots (crosses represent outliers) representing the displacement of the head in the *y*-axis for stimulations at A4 and A6. The vertical displacement varied significantly with different stimulus sites. The head's target position varied more for the anterior stimulus site A4 (one-sample Chi-squared test on variance with null hypothesis that variance is 1; *P<0.05).

Journal of Experimental Biology (2020) 223, jeb221010. doi:10.1242/jeb.221010

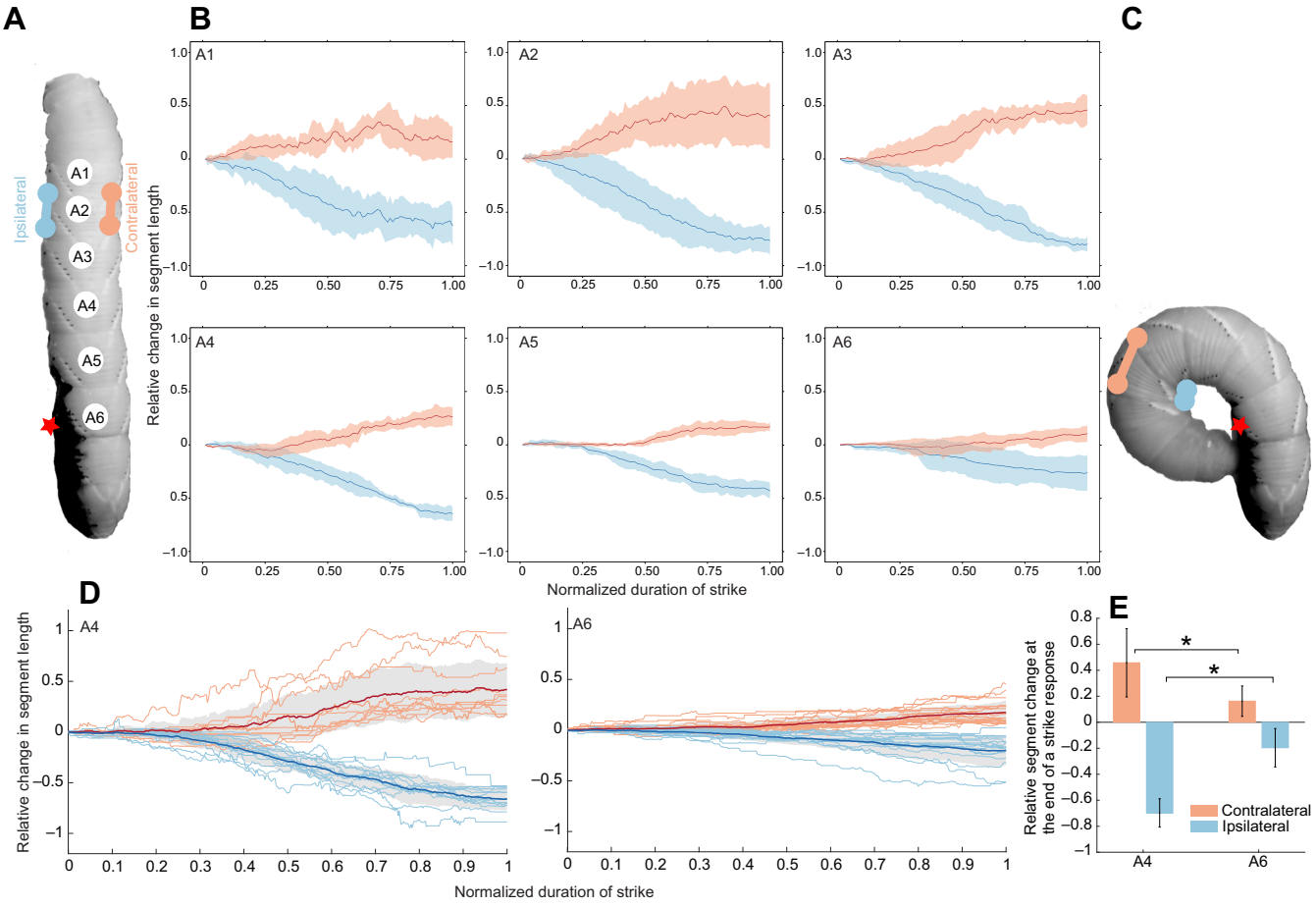

Fig. 3. Shape change of the abdominal segments during a strike response. (A) Segmental length changes were measured on the ipsilateral side (blue) and contralateral side (orange) for all abdominal segments (depicted only in abdominal segment A2 for clarity). The thermal stimulus was delivered at A6 (red star). (B) The relative change in segment length was measured for all abdominal segments from A1 to A6 (n=4 animals) and strike duration was normalized to the start of movement at 0 and the end of a strike at 1. (C) The end of the strike was marked by the head touching the target site (red star). The segmental length change on the ipsilateral (blue) and contralateral (orange) is shown only in A2 for clarity. (D) The relative change in segment length of A4 and A6 that was used for further analysis. (E) Abdominal segment A4 underwent a greater length change than A6 ipsilaterally and contralaterally (estimated marginal means Tukey method, *P<0.05; n=13 A4 ipsilateral, n=11 A4 contralateral, n=16 A6 ipsilateral, n=19 A6 contralateral, n=13 animals in D and E).

The binned probability of spike occurrence distributions was converted to smoothed functions to analyze them temporally with the kinematic changes in segment length (Fig. 5).

Relationship of EMG activity patterns with kinematics of the strike response

The speed at which a segment contracted or expanded depended linearly on its corresponding EMG spike probability distributions of both ipsilateral and contralateral sides (Table 1). GLMMs were run for all four recording sites. For segment A4, both ipsilateral and contralateral EMG probability distributions were significant predictor variables but their interaction (A4 contralateral×A4 ipsilateral) was not significant (confirmed by LR test of additive versus interaction model: A4 contralateral χ^2=0.1693, d.f.=1, P=0.6807; A4 ipsilateral χ^2=2.0743, d.f.=1, P=0.1498) (Table 1). Ipsilateral and contralateral EMG probability distributions were statistically supported parameters determining the speed of shape change of A4 (marginal LR test of relative to the full additive model; EMG A4 ipsilateral: χ^2=10.881, d.f.=1, P=0.000412, EMG A4 contralateral: χ^2=12.477, d.f.=1, P=0.02065). Similarly for segment A6, the additive model estimated the speed of expansion or contraction more parsimoniously than the interaction model (confirmed by LR test of additive versus interaction model: A6 contralateral χ^2=0.9626, d.f.=1, P=0.3265; A6 ipsilateral χ^2=2.1452, d.f.=1, P=0.143). But, only the ipsilateral EMG probability distribution contributed significantly towards the speed of shape change of A6 (Kinematic expansion$_{A6Contralateral}$~additive model versus EMG$_{A6Ipsilateral}$: dAIC=1.3; Kinematic expansion$_{A6Ipsilateral}$~additive model versus EMG$_{A6Ipsilateral}$: dAIC=0.7; when both models are winning if they are within 2 dAICs and so the most parsimonious is selected, i.e. speed of shape change of A6~EMG$_{A6Ipsilateral}$).

The ipsilateral and contralateral kinematic profiles of either abdominal segments were driven strongly by their corresponding ipsilateral muscle activity. The contralateral muscle activity was a smaller predictor variable for the speed of contraction and expansion for both segments and was significant for abdominal segment A4 (Table 1).

Central spike trains

Although spike trains recorded from the same muscle varied from trial to trial, the temporal structure across multiple responses can be represented as a central spike train using a function mapping and averaging algorithm (Julienne and Houghton, 2013). The central spike trains for each side of A4 and A6 were generated using

Journal of Experimental Biology (2020) 223, jeb221010. doi:10.1242/jeb.221010

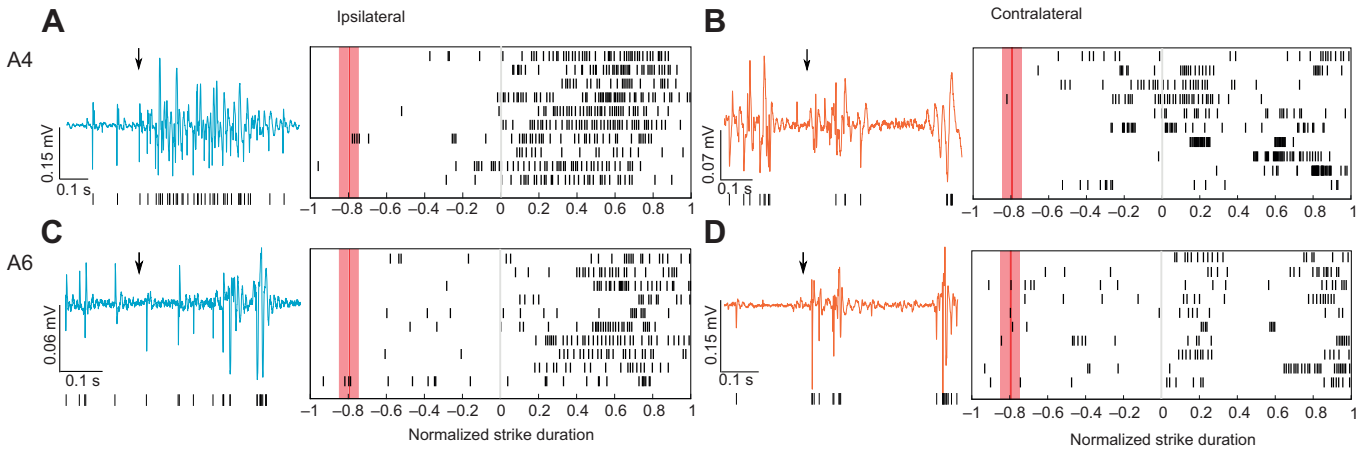

Fig. 4. EMG data from all four recording sites. (A) A4 ipsilateral. (B) A4 contralateral. (C) A6 ipsilateral. (D) A6 contralateral. Left: example EMG trace, which was converted to a raster of neural spikes (shown below). Arrows indicate when the strike was initiated. Right: EMG data from all analyzed strike responses were converted to neural spikes and normalized to their respective strike duration. The average onset of the laser stimulus was at −0.7972±0.0543 (mean±s.e.m., marked on EMG rasters in red with mean shown as a dark red line). The start of the strike response at 0 is marked by a gray line running across all the rasters and the end of the strike is at 1. Each individual example EMG trace represents a portion of the bottom-most EMG raster shown in all boxes.

τ=0.001 in the decaying exponential kernel. Given a collection of spike trains for each recording site (n=13 A4 ipsilateral, n=11 A4 contralateral, n=16 A6 ipsilateral, n=19 A6 contralateral), the filtering produced a collection of functions that were averaged to make a function average. The central spike train was obtained by minimizing and optimizing the square error between the function average and the filtered spike train using a greedy algorithm (Julienne and Houghton, 2013). The resultant spike trains illustrate

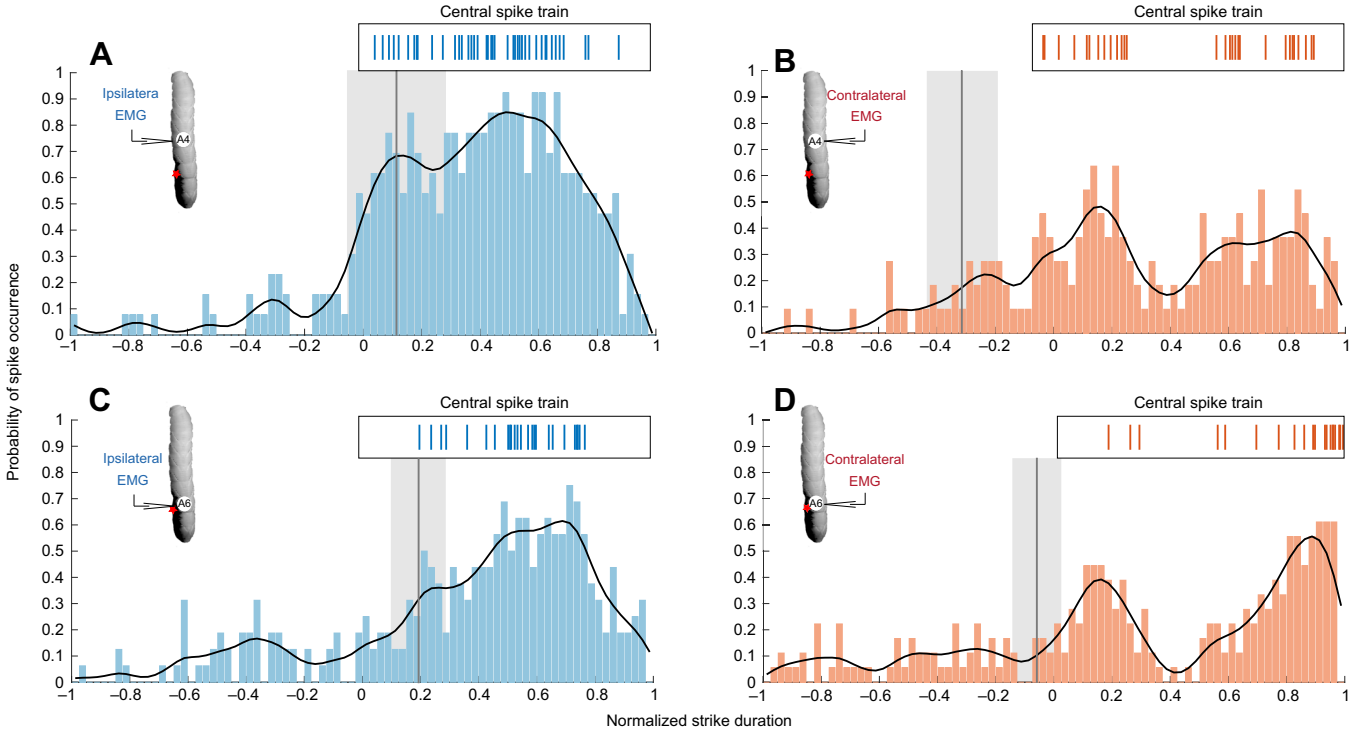

Fig. 5. Rasters with neural spikes from all four recording sites converted into binned spike probability distributions. The thermal stimulus was delivered at A6 (red star). The probability of spike occurrence was binned into 80 time intervals and normalized to the strike duration. The bins were fitted to a smoothing spline fit for (A) A4 ipsilateral, smoothing parameter λ=0.0007, R^2=0.943, sum of squares error=0.478; (B) A4 contralateral, λ=0.0007, R^2=0.72, sum of squares error=0.623; (C) A6 ipsilateral, λ=0.0007, R^2=0.842, sum of squares error=0.55; (D) A6 contralateral, λ=0.0007, R^2=0.801, sum of squares error=0.430. The average start of EMG activity normalized to the duration of the strike response was as follows: A4 ipsilateral 0.1188±0.1688 (mean±s.e.m. marked in gray with mean shown by a black line: n=13 A4 ipsilateral), A4 contralateral −0.3187±0.1187 (n=11 A4 contralateral), A6 ipsilateral 0.1937±0.092 (n=16 A6 ipsilateral) and A6 contralateral −0.0688±0.082 (n=19 A6 contralateral). The insets represent the central spike trains for each recording site obtained from running an averaging algorithm across all the rasters (n=13 A4 ipsilateral, n=11 A4 contralateral, n=16 A6 ipsilateral, n=19 A6 contralateral). The central spike trains have been temporally aligned to their corresponding normalized strike durations.

Journal of Experimental Biology (2020) 223, jeb221010. doi:10.1242/jeb.221010

Table 1. Summary information about the linear model of the dependent variable, kinematic speed of the relative change in segment length (expansion and contraction), on the predictor smoothed neural spike probability curves (called EMG) of both sides of the corresponding segment

Kinematic speed	*n*	α (EMG ipsilateral)	ANOVA of α (*P*-value)	β (EMG ipsilateral)	ANOVA of β (*P*-value)	*F*-statistic	R^2
A4 contralateral expansion speed	11	0.0354**	0.0077	−0.0256*	0.0227	7.053; *P*=0.0025	0.276
A4 ipsilateral contraction speed	13	0.03145***	8.53e-06	−0.0430**	0.0025	16.67; *P*=6.9e−06	0.474
A6 contralateral expansion speed	19	0.01259**	0.00293	0.00674	0.1144	5.091; *P*=0.0111	0.2158
A6 ipsilateral contraction speed	16	0.01498***	0.00024	0.00677	0.0901	8.249; *P*=0.0011	0.3084

n, total number of strike responses. Contralateral expansion speed=α(EMG ipsilateral)+β(EMG contralateral)+intercept; ipsilateral contraction speed=α(EMG ipsilateral)+β(EMG contralateral)+intercept. For segment A4, both ipsilateral and contralateral EMG probability distributions were significant predictor variables for the speed of expansion and contraction. The ipsilateral EMG distribution has a positive effect while the contralateral EMG distribution has a negative effect on the speed of A4's shape change. For segment A6, only the ipsilateral EMG probability distribution has a significant and positive contribution towards the speed of shape change of the segment. *P<0.05, **P<0.01, ***P<0.001.

the sporadic nature of the contralateral muscle activation compared with that on the ipsilateral side, and a phase delay (approximately 0.2 of the normalized spike duration) of the A6 body segment compared with A4 (Fig. 6). The central spike train on the contralateral side showed a distinctive pause in firing between 0.3 and 0.5 of strike duration which preceded the fastest rate of segment expansion on that side.

DISCUSSION

Thermally evoked nocifensive strike response in caterpillars is targeted to the stimulus

Strike behavior is a useful system for studying the neuromechanics of a fast movement in a soft animal. In response to mechanical stimuli, such as a sharp pinch, the caterpillar's response is variable, including partial strikes (in which the head does not reach the stimulus site) and stronger responses such as thrashing from side to side (Walters et al., 2001). We have found that strike behavior can be evoked using a noxious thermal stimulus produced by an IR laser. With the laser, it is easier to control the magnitude, location and duration of thermal stimuli. The evoked movements are also more consistent and reproducible than those produced by poking.

As with the response to mechanical stimuli (van Griethuijsen et al., 2013), strikes to dorsal laser stimuli were less accurate than those to ventral stimuli and strikes to posterior stimuli were more accurate than those to anterior segments. Also, in keeping with previously described responses to mechanical stimuli, the initial contact point was generally posterior to the stimulus site and the mandibles were scraped anteriorly across the stimulus site. Because a thermal stimulus does not mechanically interfere with subsequent movements, the head trajectory and movements of individual body segments can be tracked accurately. Regardless of the stimulation site (A4 or A6), the strike trajectories had similar starting angles, but they diverged approximately halfway through the movement to target the stimulus. This strongly suggests that strikes are actively controlled rather than a ballistic 'throwing' of the head towards its target. For the head to reach different target sites, the segments must shorten to different extents. The different strike trajectories following stimulation of A4 or A6 are presumably produced by modulating activity in the anterior segments to target the strikes along the anterior–posterior axis.

Mechanical considerations

Many hydrostatic animals such as mollusks and annelids use internal pressure changes generated by muscles to move parts of their body very quickly. Using fiber reinforced tissues and incompressible, constant-volume body compartments, they can produce extreme changes in shape or very fast displacements (Wainwright, 1988). For example, minute changes in the diameter of the squid arm generate an explosive change in length that is used to catch its prey within 30 ms (Kier, 1982). However, caterpillars do not undergo such massive changes in shape, and it is unlikely that they use pressure changes to generate fast movements. In previous work, we characterized the active and passive mechanical properties of *M. sexta* muscles (Woods et al., 2008) and showed that the body wall is strongly anisotropic (Lin et al., 2009). We also derived constitutive equations for both tissues (Dorfmann et al., 2007, 2008;

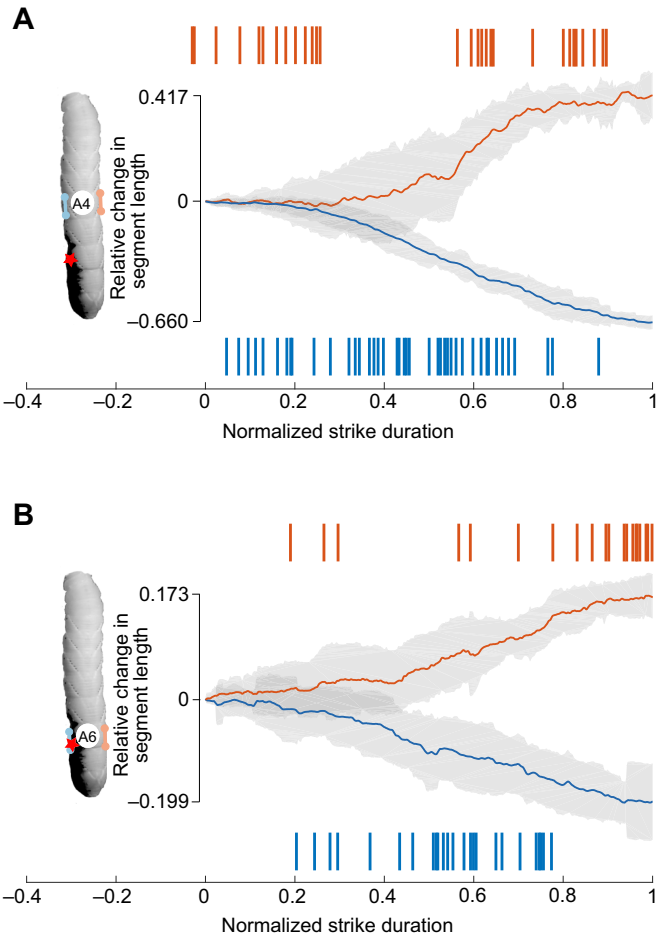

Fig. 6. Relative abdominal segment length changes. (A) A4. (B) A6. Changes are temporally aligned to the normalized strike duration and the corresponding central spike train (using rasters from *n*=13 A4 ipsilateral, *n*=11 A4 contralateral, *n*=16 A6 ipsilateral, *n*=19 A6 contralateral) (Fig. 5). The segmental length changes were measured on the ipsilateral side (in blue) and contralateral side (in orange). The thermal stimulus was delivered at A6 (red star).

Paetsch et al., 2012) and used these to model the relationship between body size, internal pressure and body stiffness (Lin et al., 2011). This model showed that increasing body pressure beyond the low levels found in *M. sexta* does little to increase relative body stiffness and it places constraints on cuticle thickness and muscle surface area. Additional studies on the morphology of *M. sexta* during crawling (Trimmer and Issberner, 2007) show that body segments do not expand circumferentially when they shorten so they do not maintain constant volume but instead displace tissues and fluid dynamically. This movement of tissues has also been confirmed by high-energy x-ray videography (Simon et al., 2010b). All these considerations make it unlikely that rapid strike movements are generated by hydrostatic mechanisms but do not discount the possibility that there are contributions from pressure changes and elastic energy storage in other tissues.

Ipsilateral muscle activity drives the strike response

During a strike, a wave of abdominal movements proceeded posteriorly with delays between the onset of strike (head movements) and segment movement increasing from about 30 ms in A1 to 200 ms in A6. EMG activity preceded movements in the corresponding segment, which may be due to excitation–contraction delays. Because segmental movements are a complex aggregate of activity in multiple muscles it is difficult to predict the expected delays. Isolated *M. sexta* muscles stimulated at 20 Hz reach 80% of their maximum force in 0.56 s (Woods et al., 2008), which is similar to that measured for segment shortening by longitudinal muscles during crawling (Simon et al., 2010a) and for proleg retraction by the principal planta retractor muscle (Mukherjee et al., 2018). We presume that segment shortening during a strike is subject to similar delays, which is why an increase in ipsilateral EMG activity in segment A4 precedes any detectable shortening by about 130 ms (~25% of mean strike duration). This effect was not evident in segment A6, but this segment does not shorten much, and EMG activity was much lower than for segment A4. The ipsilateral EMG activity was continuous and coincided with a progressive contraction of the ipsilateral side of the segment. Although the speed of length changes must be affected by the combined activity of both ipsilateral and contralateral muscles, the contractions and expansions were not symmetrical. Furthermore, the different activity patterns on each side suggest that the muscles serve roles other than simple right–left antagonism. As expected, the speed of length changes was correlated with the frequency of the muscle stimulation, suggesting that ipsilateral muscle activity drives the strike response. This is consistent with the ipsilateral muscles providing most of the energy for rapid curling of the body.

Contralateral muscle activity – a role in stability control?

During a strike, the contralateral muscle activity was episodic, concentrated only at the beginning and the end of the strike response. This activity did not correspond directly with movement, which suggests a role for contralateral muscles in resisting the ipsilateral muscles and stabilizing the body. Measurements of the contralateral EMG start times showed that there was a small increase in contralateral muscle activation before the head began to move (negative start times), even in the more posterior A4 and A6 body segments. It is possible that simultaneous activity of ipsilateral and contralateral muscles at the beginning of the segment movement is important for deciding the direction of the strike: both sets of muscles are initially activated, and then ipsilateral activity overcomes and drives the movement in its direction.

The decline of contralateral muscle activity in the middle of the strike response occurred immediately before a rapid expansion phase of the contralateral side. In segment A4, the lag between burst cessation and an increased expansion rate was approximately 160 ms (~30% of the mean strike duration), which is consistent with the expected delay between a change in the EMG and the muscle force. However, segmental shape changes will be determined by the activity of multiple muscles in each segment and by those in adjacent segments, so it is unlikely that expansion is mediated by contralateral inhibition alone.

Subsequent activation of the contralateral muscle at the end of a strike may be involved in controlling contact with the body or even preparing to reverse the movement and reset the body posture. This late activity is particularly intense in segment A6, which would be subject to the highest tension and would require the highest forces to straighten the abdomen.

Movement encoding by variable spike trains

A remarkable feature of muscle activation underlying the strike behavior is the variability of individual EMG responses. No two spike trains were the same and the distribution of spikes was broad compared with the consistent movements themselves. Similar variability in *M. sexta* muscle activation has been described previously in the DIM muscles during crawling (Metallo and Trimmer, 2015) and in the principal planta retractor muscle during proleg withdrawal (Mukherjee et al., 2018). This contrasts with the tight spike timing and movement relationships often described for locomotion in articulated animals such as cockroaches, locusts and vertebrates (Grillner and El Manira, 2020; Page et al., 2008; Watson and Ritzmann, 1997) and for flight control in adult *M. sexta* (Sober et al., 2018). Presumably, many other muscles contribute to the control of strike behavior and it is the coordination of activity in these muscle groups that dictates the precision of the movement, rather than the activation of DIM alone.

Here, we show that despite the high variability of recorded spike trains, the average spike probability distributions reveal differences in the ipsilateral and contralateral motor patterns underlying the bending movement. However, averaging over multiple trials with differences in spike timing and spike number could lead to the loss of important features common across all trials. Therefore, to get a better representation of the temporal structure of the spike trains, we used a mathematically rigorous algorithm to calculate the ‘central spike train’ (Julienne and Houghton, 2013). In this method, each neural raster is converted into a function and these functions are averaged using a greedy algorithm to efficiently minimize the error and to ensure that the central spike train also lies on the space of functions. This approach demonstrated clearly that ipsilateral spikes occur throughout the movement, with a cluster of increased firing approximately halfway through the strike. In contrast, contralateral spikes rarely occur in the middle of a strike movement but are instead concentrated at the start and end of a strike. This confirms our findings from the average spike probability distributions and reinforces the notion that strike behavior is an actively controlled and coordinated motor pattern.

Acknowledgements

We would like to thank Dr Conor Houghton for supplying us with the code to carry out the central spike train analyses.

Competing interests

The authors declare no competing or financial interests.

Author contributions

Conceptualization: R.M., B.A.T.; Methodology: R.M.; Software: R.M., T.E.; Validation: R.M.; Formal analysis: R.M., T.E.; Investigation: R.M.; Resources: B.A.T.; Writing - original draft: R.M.; Writing - review & editing: R.M., D.P.C., B.A.T.; Visualization: R.M., D.P.C.; Supervision: B.A.T.; Project administration: B.A.T.; Funding acquisition: B.A.T.

Funding

This work was supported by grants from the Army Research Office [W911NF1610095], the National Science Foundation Biological Science Directorate [IOS-1456471] and the National Science Foundation Integrative Graduate Education and Research Training [DGE-IGERT-1144591] to B.A.T.

Supplementary information

Supplementary information available online at https://jeb.biologists.org/lookup/doi/10.1242/jeb.221010.supplemental

References

Aubert, X., Roquet, M. L. and Van der Elst, J. (1951). The tension-length diagram of the frog's sartorius muscle. *Arch. Int. Physiol.* **59**, 239-241. doi:10.3109/13813455109145002

Bates, D., Mächler, M., Bolker, B. and Walker, S. (2015). Fitting linear mixed-effects models using lme4. *Stat. Soft.* **67**, 1406.5823. doi:10.18637/jss.v067.i01

Bell, R. A. and Joachim, F. A. (1978). Techniques for rearing laboratory colonies of tobacco hornworms and pink bollworms. *J. Stat. Soft* **67**, doi:10.18637/jss.v067.i01

Colobert, B., Crétual, A., Allard, P. and Delamarche, P. (2006). Force-plate based computation of ankle and hip strategies from double-inverted pendulum model. *Clin. Biomech.* **21**, 427-434. doi:10.1016/j.clinbiomech.2005.12.003

Dominick, O. S. and Truman, J. W. (1986). The physiology of wandering behaviour in Manduca sexta. III. Organization of wandering behaviour in the larval nervous system. *J. Exp. Biol.* **121**, 115-132.

Dorfmann, A., Trimmer, B. A. and Woods, W. A., Jr. (2007). A constitutive model for muscle properties in a soft-bodied arthropod. *J. R Soc. Interface* **4**, 257-269. doi:10.1098/rsif.2006.0163

Dorfmann, A. L., Woods, W. A. and Trimmer, B. A. (2008). Muscle performance in a soft-bodied terrestrial crawler: constitutive modelling of strain-rate dependency. *J. R Soc. Interface* **5**, 349-362. doi:10.1098/rsif.2007.1076

Elliott, C., Vijayakumar, V., Zink, W. and Hansen, R. (2007). National instruments LabVIEW: a programming environment for laboratory automation and measurement. *JALA* **12**, 17-24. doi:10.1016/j.jala.2006.07.012

Fox, J., Friendly, M. and Weisberg, S. (2013). Hypothesis tests for multivariate linear models using the car package. *The R Journal* **5**, 39-52. doi:10.32614/RJ-2013-004

Frings, H. (1945). The reception of mechanical and thermal stimuli by caterpillars. *J. Exp. Zool.* **99**, 115-140. doi:10.1002/jez.1400990302

Grillner, S. and El Manira, A. (2020). Current principles of motor control, with special reference to vertebrate locomotion. *Physiol. Rev.* **100**, 271-320. doi:10.1152/physrev.00015.2019

Holmes, P., Full, R. J., Koditschek, D. and Guckenheimer, J. (2006). The dynamics of legged locomotion: models, analyses, and challenges. *SIAM Rev.* **48**, 207-304. doi:10.1137/S0036144504445133

Julienne, H. and Houghton, C. (2013). A simple algorithm for averaging spike trains. *J. Math. Neurosci.* **3**, 3. doi:10.1186/2190-8567-3-3

Kier, W. M. (1982). The functional morphology of the musculature of squid (Loliginidae) arms and tentacles. *J. Morphol.* **172**, 179-192. doi:10.1002/jmor.1051720205

Kier, W. M. and Schachat, F. H. (1992). Biochemical comparison of fast- and slow-contracting squid muscle. *J. Exp. Biol.* **168**, 41-56.

Kier, W. M. and Smith, K. K. (1983). The biomechanics of movement in tongues and tentacles. *J. Biomech.* **16**, 292-293. doi:10.1016/0021-9290(83)90176-8

Kier, W. M. and Smith, K. K. (1985). Tongues, tentacles and trunks: the biomechanics of movement in muscular-hydrostats. *Zool. J. Linn. Soc.* **83**, 307-324. doi:10.1111/j.1096-3642.1985.tb01178.x

Kier, W. M. and Stella, M. P. (2007). The arrangement and function of octopus arm musculature and connective tissue. *J. Morphol.* **268**, 831-843. doi:10.1002/jmor.10548

Kristan, W. B., Calabrese, R. L. and Friesen, W. O. (2005). Neuronal control of leech behavior. *Prog. Neurobiol.* **76**, 279-327. doi:10.1016/j.pneurobio.2005.09.004

Levine, R. B. and Truman, J. W. (1985). Dendritic reorganization of abdominal motoneurons during metamorphosis of the moth, Manduca sexta. *J. Neurosci.* **5**, 2424-2431. doi:10.1523/JNEUROSCI.05-09-02424.1985

Lin, H.-T., Dorfmann, A. L. and Trimmer, B. A. (2009). Soft-cuticle biomechanics: a constitutive model of anisotropy for caterpillar integument. *J. Theor. Biol.* **256**, 447-457. doi:10.1016/j.jtbi.2008.10.018

Lin, H.-T., Slate, D. J., Paetsch, C. R., Dorfmann, A. L. and Trimmer, B. A. (2011). Scaling of caterpillar body properties and its biomechanical implications for the use of a hydrostatic skeleton. *J. Exp. Biol.* **214**, 1194-1204. doi:10.1242/jeb.051029

McMackin, M. Z., Lewin, M. R., Tabuena, D. R., Arreola, F. E., Moffatt, C. and Fuse, M. (2016). Use of von Frey filaments to assess nociceptive sensitization in the hornworm, Manduca sexta. *J. Neurosci. Methods* **257**, 139-146. doi:10.1016/j.jneumeth.2015.09.015

Metallo, C. and Trimmer, B. A. (2015). Silk coating as a novel delivery system and reversible adhesive for stiffening and shaping flexible electrodes. *J. Biol. Method.* **2**, e13. doi:10.14440/jbm.2015.41

Mezoff, S., Papastathis, N., Takesian, A. and Trimmer, B. A. (2004). The biomechanical and neural control of hydrostatic limb movements in Manduca sexta. *J. Exp. Biol.* **207**, 3043-3053. doi:10.1242/jeb.01136

Mukherjee, R. and Trimmer, B. A. (2019). Local and generalized sensitization of thermally evoked defensive behavior in caterpillars. *J. Comp. Neurol.* **528**, 805-815. doi:10.1002/cne.24797

Mukherjee, R., Vaughn, S. and Trimmer, B. A. (2018). The neuromechanics of proleg grip release. *J. Exp. Biol.* **221**, jeb173856. doi:10.1242/jeb.173856

Nishikawa, K. C., Kier, W. M. and Smith, K. K. (1999). Morphology and mechanics of tongue movement in the African pig-nosed frog Hemisus marmoratum: a muscular hydrostatic model. *J. Exp. Biol.* **202**, 771-780.

Paetsch, C., Trimmer, B. A. and Dorfmann, A. (2012). A constitutive model for active-passive transition of muscle fibers. *Int. J. Non-Linear Mech.* **47**, 377-387. doi:10.1016/j.ijnonlinmec.2011.09.024

Page, K. L., Zakotnik, J., Dürr, V. and Matheson, T. (2008). Motor control of aimed limb movements in an insect. *J. Neurophysiol.* **99**, 484-499. doi:10.1152/jn.00922.2007

Patek, S. N., Dudek, D. M. and Rosario, M. V. (2011). From bouncy legs to poisoned arrows: elastic movements in invertebrates. *J. Exp. Biol.* **214**, 1973-1980. doi:10.1242/jeb.038596

Quillin, K. J. (1998). Ontogenetic scaling of hydrostatic skeletons: geometric, static stress and dynamic stress scaling of the earthworm Lumbricus terrestris. *J. Exp. Biol.* **201**, 1871-1883.

Ruiz, S., Or, D. and Schymanski, S. J. (2015). Soil penetration by earthworms and plant roots—mechanical energetics of bioturbation of compacted soils. *PLoS ONE* **10**, e0128914. doi:10.1371/journal.pone.0128914

Simon, M. A., Fusillo, S. J., Colman, K. and Trimmer, B. A. (2010a). Motor patterns associated with crawling in a soft-bodied arthropod. *J. Exp. Biol.* **213**, 2303-2309. doi:10.1242/jeb.039206

Simon, M. A., Woods, W. A., , Jr, Serebrenik, Y. V., Simon, S. M., van Griethuijsen, L. I., Socha, J. J., Lee, W.-K. and Trimmer, B. A. (2010b). Visceral-locomotory pistoning in crawling caterpillars. *Curr. Biol.* **20**, 1458-1463. doi:10.1016/j.cub.2010.06.059

Skierczynski, B. A., Wilson, R. J. A., Kristan, W. B., , Jr. and Skalak, R. (1996). A model of the hydrostatic skeleton of the leech. *J. Theor. Biol.* **181**, 329-342. doi:10.1006/jtbi.1996.0135

Sober, S. J., Sponberg, S., Nemenman, I. and Ting, L. H. (2018). Millisecond spike timing codes for motor control. *Trends Neurosci.* **41**, 644-648. doi:10.1016/j.tins.2018.08.010

Tabuena, D. R., Solis, A., Geraldi, K., Moffatt, C. A. and Fuse, M. (2017). Central neural alterations predominate in an insect model of nociceptive sensitization. *J. Comp. Neurol.* **525**, 1176-1191. doi:10.1002/cne.24124

Trimmer, B. and Issberner, J. (2007). Kinematics of soft-bodied, legged locomotion in Manduca sexta larvae. *Biol. Bull.* **212**, 130-142. doi:10.2307/25066590

van Griethuijsen, L. I., Banks, K. M. and Trimmer, B. A. (2013). Spatial accuracy of a rapid defense behavior in caterpillars. *J. Exp. Biol.* **216**, 379-387. doi:10.1242/jeb.070896

Wainwright, S. A. (1988). *Axis and Circumference*. Cambridge, Massachusetts: Harvard University Press.

Walters, E., Illich, P., Weeks, J. and Lewin, M. (2001). Defensive responses of larval Manduca sexta and their sensitization by noxious stimuli in the laboratory and field. *J. Exp. Biol.* **204**, 457-469.

Watson, J. T. and Ritzmann, R. E. (1997). Leg kinematics and muscle activity during treadmill running in the cockroach, Blaberus discoidalis: II. Fast running. *J. Comp. Physiol. A* **182**, 23-33. doi:10.1007/s003590050154

Westneat, M. W., Hale, M. E., Mchenry, M. J. and Long, J. H. (1998). Mechanics of the fast-start: muscle function and the role of intramuscular pressure in the escape behavior of amia calva and polypterus palmas. *J. Exp. Biol.* **201**, 3041-3055.

Wilson, R. J., Skierczynski, B. A., Blackwood, S., Skalak, R. and Kristan, W. B., Jr. (1996). Mapping motor neurone activity to overt behaviour in the leech: internal pressures produced during locomotion. *J. Exp. Biol.* **199**, 1415-1428.

Woods, W. A., , Jr., Fusillo, S. J. and Trimmer, B. A. (2008). Dynamic properties of a locomotory muscle of the tobacco hornworm Manduca sexta during strain cycling and simulated natural crawling. *J. Exp. Biol.* **211**, 873-882. doi:10.1242/jeb.006031

Yekutieli, Y., Sagiv-Zohar, R., Aharonov, R., Engel, Y., Hochner, B. and Flash, T. (2005). Dynamic model of the octopus arm. I. Biomechanics of the octopus reaching movement. *J. Neurophysiol.* **94**, 1443-1458. doi:10.1152/jn.00684.2004

Zeileis, A. and Hothorn, T. (2002). Diagnostic checking in regression relationships. R News 2, 7-10. https://CRAN.R-project.org/doc/Rnews/

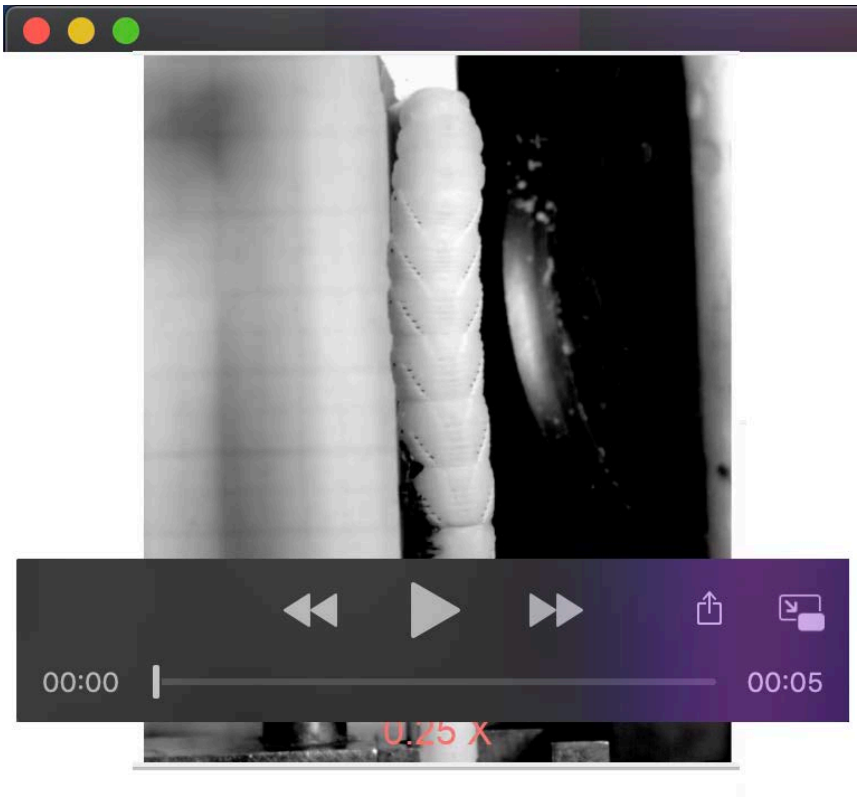

Movie 1. An example video of the strike response. The video exemplifies a strike response with a description of the muscle activity in two segments, A4 and A6. The ipsilateral and contralateral sites are marked by buttons on the corners of the video and they turn on when the muscles in that segment site activate during the strike response. The timing of the activity of each button corresponds to its corresponding central spike train (Results section, Central spike trains that represent the average activity patterns in A4 and A6 during a strike response) that represent the average firing patterns of the segments. The video shows the differences in co-activation of muscles on each side of the body and anterior-posterior phase delays.